Joint International Topical Meeting on Mathematics & Computation and Supercomputing in Nuclear Applications (M&C + SNA 2007)
Monterey, California, April 15-19, 2007, on CD-ROM, American Nuclear Society, La Grange Park, IL (2007)

NEW CAPABILITIES IN MERCURY: A MODERN, MONTE CARLO PARTICLE TRANSPORT CODE

Richard Procassini, Dermott Cullen, Gregory Greenman, Christian Hagmann,
Kevin Kramer, Scott McKinley, Matthew O'Brien and Janine Taylor

Lawrence Livermore National Laboratory
Mail Stop L-95, P.O. Box 808
Livermore, CA 94551
United States of America

spike@llnl.gov, cullen1@llnl.gov, greenman1@llnl.gov, cah@llnl.gov,
kramer12@llnl.gov, quath@llnl.gov, mobrien@llnl.gov, taylorj@llnl.gov

ABSTRACT

The new physics, algorithmic and computer science capabilities of the **Mercury** general-purpose Monte Carlo particle transport code are discussed. The new physics and algorithmic features include in-line energy deposition and isotopic depletion, significant enhancements to the tally and source capabilities, diagnostic ray-traced particles, support for multi-region hybrid (mesh and combinatorial geometry) systems, and a probability of initiation method. Computer science enhancements include a second method of dynamically load-balancing parallel calculations, improved methods for visualizing 3-D combinatorial geometries and initial implementation of an in-line visualization capabilities.

Key Words:Monte Carlo methods, particle transport, parallel computing

1. INTRODUCTION

An update on the development of the **Mercury** Monte Carlo particle transport code [1], [2] is presented. **Mercury** is a modern, general-purpose Monte Carlo code being developed at the Lawrence Livermore National Laboratory (LLNL). The nuclear data interface and collisional kinematics capabilities in **Mercury** are provided by the Monte Carlo All-Particle Method (**MCAPM**) library [3]. Several important capabilities have been added to both **Mercury** and **MCAPM** during the past year. Most of the effort has been concentrated in the area of physics and algorithm enhancements.

The first of these is the addition of an energy deposition and isotopic depletion capability into **Mercury**. This permits the user to tally the energy (mass) that is deposited (depleted and accreted) into any cell as a result of nuclear collisions. Both analog (collision based) and expected-value (flux based) versions of the deposition and depletion algorithms have been developed. The expected-value energy deposition feature was straightforward to implement, since the LLNL Evaluated Nuclear Data Library (ENDL) [4] data format used by **MCAPM** has always provided a multi-group energy-deposition cross section. This is defined as the reaction-weighted energy deposit to the residual reaction products

$$\sigma_{Edep} \equiv \sum_j \sigma_{r,j} E_{avail} = \sum_j \sigma_{r,j} (E_{inc} + Q_{r,j}) \quad (1)$$

where $\sigma_{r,j}$ is the reaction cross section for the *j*-th reaction, E_{avail} is the energy available for deposition to the residual reactions products, E_{inc} is the kinetic energy of the incident particle, and $Q_{r,j}$ is the energy released by (required for) the reaction. Modification of the **MCAPM** library was required to provide an expected-value continuous energy version of the energy-deposition cross section. While the mass change in a cell arising from nuclear reactions is computed and may be tallied, it is not currently accumulated and carried forward in time. Additional modifications to **Mercury** are planned that will provide support for time-dependent depletion calculations, although a capability to model the decay of radioactive isotopes is not being considered.

Extension of the previous tally and source capabilities in **Mercury** have been major efforts over the past year. These are analogous capabilities which permit the user to accumulate (tally) into, or sample (source) from, an *n*-dimensional distribution or space. The tally space is explicitly treated as a correlated distribution, while the source space is handled either as an uncorrelated or correlated distribution [5]. Each dimension of an *n*-dimensional spaces can represent time, energy, angle(s), a 2-D or 3-D Cartesian mesh, combinatorial geometry (CG) surfaces and cells, as well as numerous tally-only attributes, such as the number of collisions, particle age, creation event, creation material, etc. Support is provided for both standard tallies (particle balance, particle flux, particle spectra, energy and mass deposition and cross sections) and user-defined tallies (where the user specifies the space into which results are accumulated which triggered by specific events). A series of functional responses (translations, rotations, etc) may also be applied to the particle before its contribution to a tally is accumulated. The source capability supports a number of standard geometric shapes (point, line, cylinder, sphere, etc), energy (monoenergetic, Watt fission and various thermonuclear reactions) and temporal (impulse) distributions, as well as user-defined source distributions.

The **Mercury** tally module also forms the core of a tally post-processing tool named **Caloris**, which is named after one of the major craters on the planet Mercury. Tally data which has been written to disk during a prior **Mercury** calculation, either as particle records or as an *n*-dimensional distribution/space, can be read by **Caloris** for further processing. **Caloris** can currently process tally data by (a) collapsing the tally distribution from *N* to *M* dimensions $(N \geq M)$, and (b) filtering particles according to a set of criteria in order to develop a source for a subsequent **Mercury** transport calculation. A planned extension to both **Mercury** and **Caloris** is an in-line link to the **VisIt** [6] visualization and data analysis tool. This will permit users to visualize complex tally distributions, without having to pour over pages of printed output to gain insight from the multi-dimensional tally results. While the in-line link to **VisIt** will dramatically improve the flexibility of **Mercury** and **Caloris**, it may currently be used for the same purpose as a post processor.

A new capability which is often used in conjunction with tallies are *diagnostic* particles. These are different from *transport* particles, in that they "track" through the system via ray tracing. Diagnostic particles do *not* scatter, but simply follow a straight-line trajectory until they escape from the system. In order to account for collisional losses, the weight of the particle is exponentially attenuated as it travels along its trajectory. The preferred trajectory of a diagnostic particle can be defined from tally attributes, such as the normal vector to the image plane in an imaging

experiment. There are two types of processes that can create diagnostic particles: (a) those which result in isotropic emission of secondary particles, such as thermonuclear reactions, and (b) collisions which produce secondary particles, such as scattering, fission, capture, (n, Xn), etc.. In the latter case, **Mercury** employs a biased, directional scattering technique which has been implemented in the **MCAPM** library. This algorithm emits the secondary diagnostic particle along the preferred trajectory, but with a weight that is adjusted to account for the probabilistic difference of emitting in the preferred/biased direction, instead of in the unbiased direction.

To demonstrate the new tally and diagnostic particle capabilities in **Mercury**, consider the imaging system shown in Figure 1. The system consists of three neutron-emitting uranium components (red) in air (light green), a shield (blue) and an image plane (green). The shapes of the emitting volumes were chosen such that they could easily be discerned in the images. The results obtained using various imaging models are shown in Figure 2. Three tracking and tallying methods are shown: standard transport (top), transport augmented by rotational imaging (center) and diagnostic ray tracing (bottom). The second method uses a tally functional response in which particles with a radial distance from the symmetry axis of at least 6 cm are rotated such that their velocity components in the *x*-*z* plane are aligned along the *x*-axis (normal to the imaging plane). Note that outside of this cylindrical volume, the transport results are deliberately biased in order to create a crisper image at the image plane. Therefore, other tally results outside of that cylindrical volume, such as energy deposition in the shield region, are less accurate than those obtained

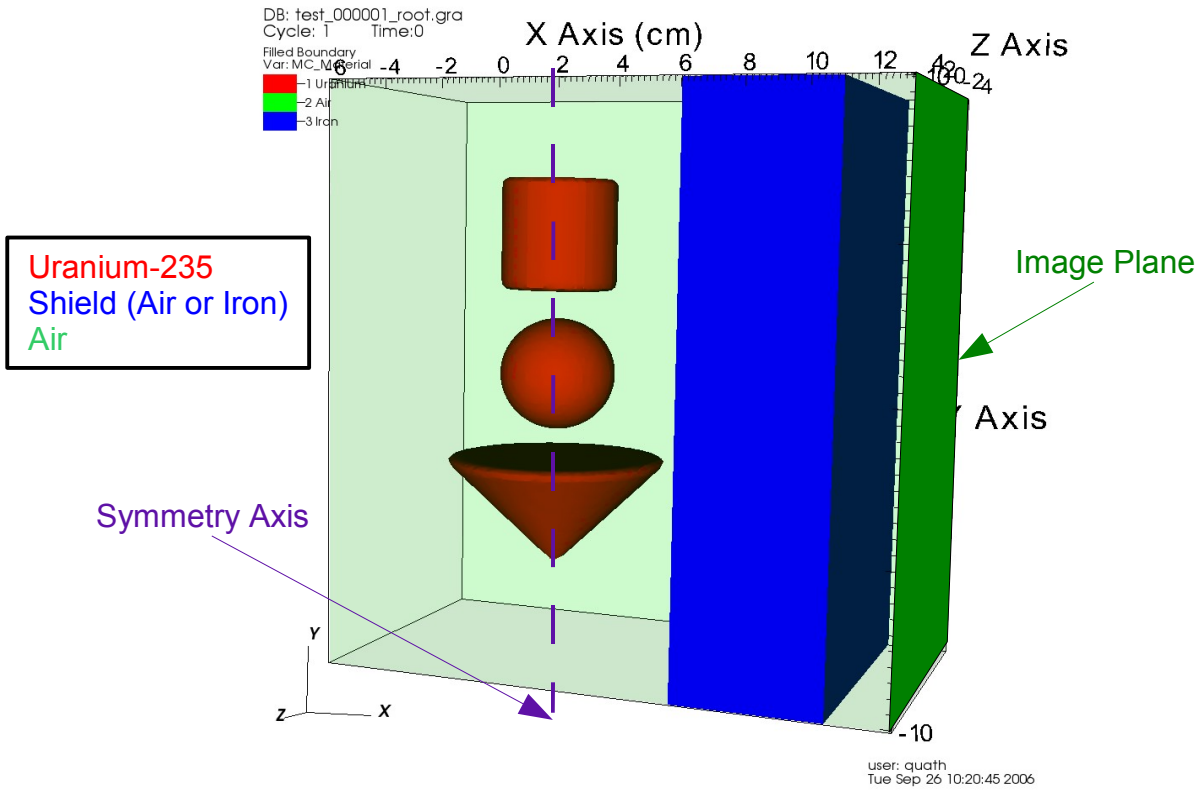

Figure 1. The geometry of the imaging system used to demonstrate of tallies. The neutron-emitting uranium components are red, the air is light green, the shield material (either air or iron) is blue, and the image plane is green.

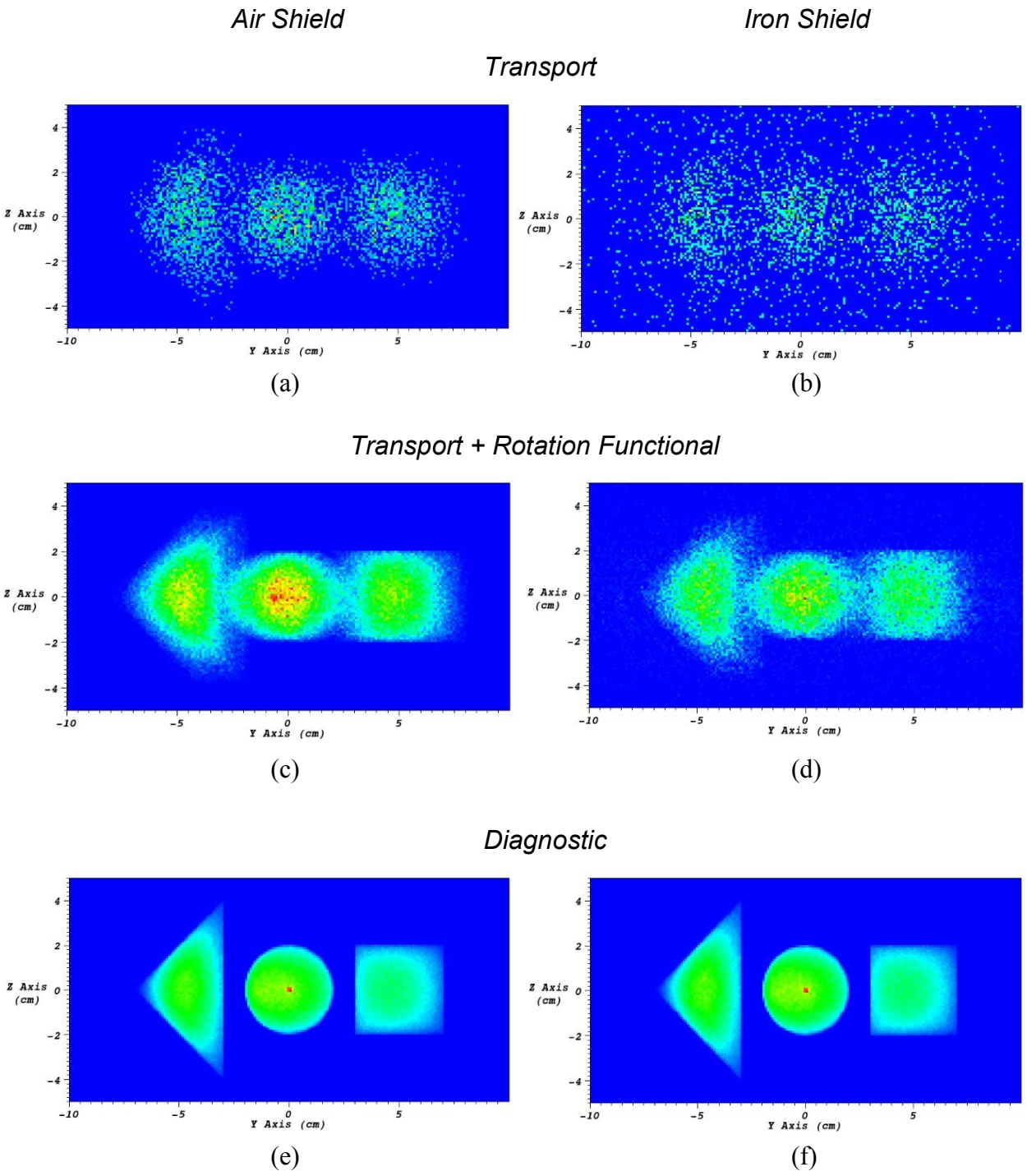

Figure 2. Neutron tally images for the imaging system shown above. The images were generated using two different shield materials (air on the left and iron on the right), as well as three different tracking/tallying methods (standard transport on the top, transport plus rotational imaging in the center, and diagnostic ray tracing on the bottom). The shapes of the emitting volumes were chosen such that they could easily be discerned in the images.

from standard transport methods. Images were obtained using "shield" regions comprised of air or iron. An isotropic, point external source is placed in the center of the sphere to initiate fissions in all three uranium components.

The standard-transport tally results (Figures 2a and 2b) provide some indication of the number, location and geometric shape of the emitting volumes. The image for the air shield is reasonably correlated with the source locations, albeit with diffuse interfaces, while the image for the iron shield is rather diffuse, but at least indicates that three source volumes are used. The transport-plus-rotational-imaging tally results (Figures 2c and 2d) are a great improvement over the standard transport results. For each shield material, one is able to discern that the three emitting volumes are conical, spherical and cylindrical in nature. In addition, the image for the air shield gives a strong indication that the external source was placed at the center of the sphere. Once again, the image for the iron shield is more diffuse than that of its air counterpart. Finally, the diagnostic-particle (ray-tracing) tally results (Figures 2e and 2f) give a high-fidelity representation of the emitting geometry, including where the emission is the strongest in each of the volumes. These images clearly show where the external source was located, and the image for the iron shield is comparable in quality (resolution and smearing) to the image for the air shield.

Another new feature of **Mercury** is the ability to track particles through hybrid, multi-region geometries. This permits the user to embed a mesh region within a three-dimensional combinatorial geometry (CG) region , which can provide a greater degree of geometric flexibility and computational efficiency. For example, this new method supports the transport of particles through a two-dimensional, axisymmetric *r-z* mesh, which could be obtained from a mesh generator, as well as transporting particles through an azimuthally-varying CG region which surrounds the mesh. As particles "leak" from the mesh region, they enter the surrounding CG region, and vice versa. A significant amount of effort has been invested to develop a spatially-decomposed, load-balanced, parallel version of this hybrid particle tracker.

One example of when a hybrid, multi-region modeling scheme could be used is for simulations of an oil-well logging experiment. For these problems, a high-resolved mesh is typically used to describe the region around the "tool" (the source and detector package) and well hole, while the CG region can be used to model the rock, sand, water and oil strata at large distances from the tool, thereby minimizing the number of zones required to model the environment. Another example of a multi-region geometry is the transportation accident scenario shown in Figure 3. A General Atomics GA-4 spent fuel cask [7], containing four (idealized) pressurized water reactor (PWR) 7x7 pin fuel assemblies, lies submerged in water on the bottom of a river. The central region of the fuel cask contains a three-dimensional Cartesian mesh that is used to model the fuel assemblies, as shown in Figure 3a. Each pin cell is modeled with a 5x5 zone mesh laterally, with 10 zones axially, for a total of 49,000 zones. The remainder of the problem is modeled as a CG region, where the zones are bounded by planar, cylindrical and spherical surfaces. This technique may be used to perform efficient multi-physics simulations of this scenario. Thermal transfer and neutron transport can be modeled within the mesh region, while in the CG region only transport is modeled. A temperature boundary condition can be applied to the outside of the mesh region, thereby permitting a complicated criticality calculation which includes the effect of decay-heat transfer within the fuel assemblies.

The final physics/algorithm enhancement is the implementation of a non-adjoint method for calculating the probability of producing a sustained chain reaction, also known as initiation probability [8]. This forward transport method is a modification of a time-dependent source calcula-

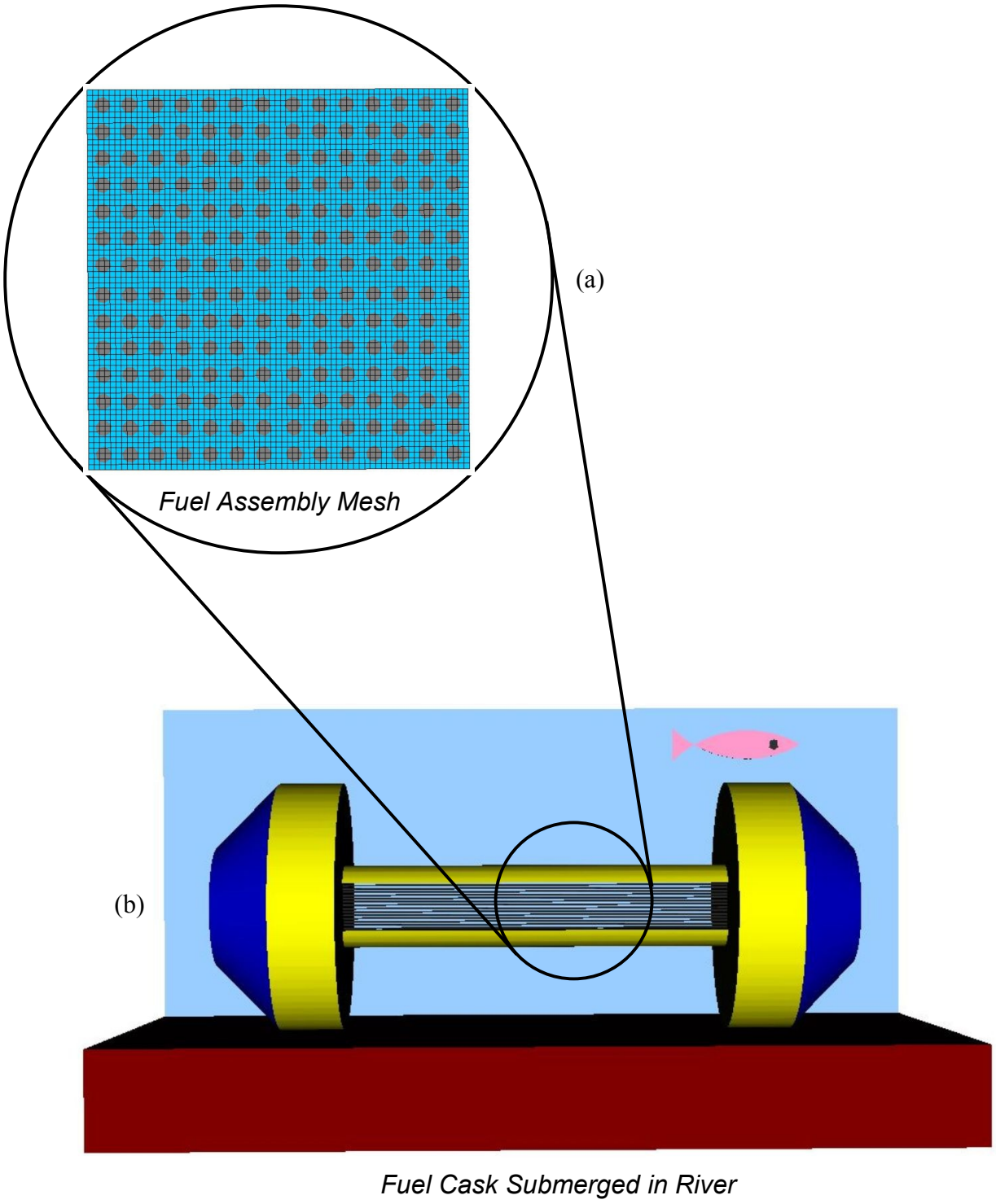

Figure 3. A hybrid, multi-region modeling technique is used to simulate a transportation accident scenario. A spent fuel cask containing four PWR fuel assemblies lies submerged in water on the bottom of a river. A three-dimensional Cartesian mesh (a) is used to model the individual pins with the fuel assemblies, while the balance of the system (b) is modeled using combinatorial geometry.

tion, where the collection source neutrons represent the progenitors of a series of neutron *families*, or *chains*. The user specifies the number of progeny neutrons required to define a divergent family/chain, as well as the maximum age for which any chain is integrated in time. The method periodically checks the number of chains that have achieved the divergence threshold, and defines the probability of initiation as the ratio of the number of divergent chains to the number of initialized chains. This method has required extension of the **MCAPM** library [3] in order to sample the *distribution* of the number of neutrons emitted in a fission event $f(\nu)$, instead of using the *average* number of neutrons emitted $\bar{\nu}$. The **MCAPM** library uses a model that is based upon the work of Terrell [9], which fits the distribution $f(\nu)$ to a Gaussian, with a width that is relatively independent of target fissile isotope.

A number of code enhancements in the area of computer science have also been included since the last in this series of meetings. A second method of load-balancing parallel transport calculations has been added to **Mercury** [10]. In contrast to the previous method [11], which dynamically varies the domain replication (the number of processors assigned to work on each domain) in response to the particle work load, this new method dynamically re-decomposes the spatial domain. This new method has been demonstrated to increase the parallel efficiency of the calculation by factors which are comparable to those achieved with the previous method.

A new CG data model has been developed for use with the **VisIt** visualization tool [6]. This new data model permits storage of the geometry as a series of analytic surfaces and the cells that are created from the aggregation of those surfaces. This new method eliminates the requirement of superimposing the CG on a structured "graphics mesh": an approach which is less accurate and which requires significantly more memory than the new method. In addition, the **VisIt** tool is currently being linked into **Mercury**. This will provide **Mercury** with an in-line graphics capability for viewing the problem geometry, as well as visualizing tallies in several modes (pseudo-color images, iso-surfaces and contour plots, etc) while the simulation is running.

While linking of **Mercury** to **VisIt** will provide users with a flexible data visualization capability, the ability to write plug-in modules for **VisIt** holds even more promise. It is our intent to develop a series of callback routines that also permits the user to validate the integrity of their problem geometry, a task which can be daunting for complicated CGs. This feature will have capabilities similar to those provided by the **TartChek** utility which is provided with the **Tart** Monte Carlo code [12]. **TartChek** can search for undefined regions of space, determine the cell and material at a given location, track particles through the system to check the validity of the CG, etc. In addition, we are investigating the use of **VisIt** as a simulation control panel. This will permit the user to visualize and certify the problem geometry, launch the simulation, and visualize the results with periodic updates in real time from within the **VisIt** GUI.

ACKNOWLEDGMENTS

This work was performed under the auspices of the U. S. Department of Energy by the University of California, Lawrence Livermore National Laboratory (LLNL) under Contract W-7405-Eng-48.

REFERENCES

1. R. J. Procassini and M. S. McKinley, "The Mercury Monte Carlo Code Web Site", Lawrence Livermore National Laboratory, Web Document UCRL-WEB-212708, http://www.llnl.gov/Mercury (2005).

2. R. J. Procassini, J. M. Taylor, M. S. McKinley, G. M. Greenman, D. E. Cullen, M. J. O'Brien, B. R. Beck and C. A. Hagmann, "Update on the Development and Validation of Mercury: A Modern, Monte Carlo Particle Transport Code", in *Proceedings of the International Topical Meeting on Mathematics and Computations*, September 12–15, 2005, Avignon, France (2005).

3. P. S. Brantley, C. A. Hagmann and J. A. Rathkopf, "MCAPM-C Generator and Collision Routine Documentation (Revision 1.2)", Lawrence Livermore National Laboratory, Report UCRL-MA-141957 (2003).

4. R. J. Howerton, D. E. Cullen, M . H. MacGregor, S. T. Perkins and E. F. Plechaty, "Integrated System For Production Of Neutronics And Photonics Calculational Constants: The LLL Evaluated Nuclear Data Library (ENDL)", Lawrence Livermore National Laboratory, Report UCRL-50400 (1976).

5. M. S. McKinley, "General Tally Support and Post-Processing in a Modern Monte Carlo Transport Code", in *Proceedings of the Joint International Topical Meeting on Mathematics & Computation and Supercomputing in Nuclear Applications*, 16 - 19 April 2007, Monterey, CA (2007).

6. The VisIt Code Team, "The VisIt Visualization Tool Web Site", Lawrence Livermore National Laboratory, Web Document UCRL-WEB-217877, http://www.llnl.gov/visit (2005).

7. A. Zimmer, J. Razvi, L. Johnson, B. Welch and D. Lancaster, "Expansion of the Capabilities of the GA-4 Legal Weight Truck Spent Fuel Shipping Cask", in *Proceedings of the PATRAM 2004 Conference*, 20 - 24 September 2004, Berlin, Germany (2004).

8. G. M. Greenman, R. J. Procassini and C. J. Clouse, "A Monte Carlo Method for Calculating Initiation Probability", in *Proceedings of the Joint International Topical Meeting on Mathematics & Computation and Supercomputing in Nuclear Applications*, 16 - 19 April 2007, Monterey, CA (2007).

9. J. Terrell, "Distributions of Fission Neutron Numbers", *Phys. Rev.*, **108**, pp. 783 - 789 (1957).

10. M. J. O'Brien, "Dynamic Load Balancing of Parallel Monte Carlo Transport Calculations via Spatial Redecomposition", in *Proceedings of the Joint International Topical Meeting on Mathematics & Computation and Supercomputing in Nuclear Applications*, 16 - 19 April 2007, Monterey, CA (2007).

11. R. J. Procassini, M. J. O'Brien and J. M . Taylor, "Load Balancing of Parallel Monte Carlo Transport Calculations", in *Proceedings of the International Topical Meeting on Mathematics and Computation, Supercomputing, Reactor Physics and Nuclear and Biological Applications*, 12 - 15 September 2005, Avignon, France (2005).

12. D. E. Cullen, "The Tart Monte Carlo Transport Code Home Page", Lawrence Livermore National Laboratory, Web Document UCRL-WEB-221645, http://www.llnl.gov/cullen1 (2005).